Capacitive Deionization using Biomass-Based Microporous Salt-Templated Heteroatom-Doped Carbons

Slawomir Porada, Florian Schipper, Mesut Aslan, Markus Antonietti, Volker Presser, and Tim-Patrick Fellinger

ChemSusChem 8(11)

Keywords:
Capacitive deionization, charge efficiency, desalination, heteroatom carbon, salt templating

Capacitive Deionization with Novel Biomass-based Microporous Salt Templated Heteroatom Carbons

Slawomir Porada,[1] Florian Schipper,[2] Mesut Aslan,[1] Markus Antonietti,[2] Volker Presser,[1,3,*] Tim-Patrick Fellinger[2,*]

Abstract: Microporous carbons are an interesting material for electrochemical applications. In this study, we evaluate several such carbons without/with N or S doping in regards to the capacitive deionization. For this purpose we extent the recent salt templating synthesis towards biomass precursors and S doped microporous carbons. The sample with the largest specific surface area (2830 m^2/g) showed 1.0 mass% N and exhibited a high salt sorption capacity of 15.0 mg/g at 1.2 V in 5 mM aqueous NaCl. While being a promising material from an equilibrium performance point of view, our study also gives first insights to practical limitations of carbon heteroatom materials. We show that high heteroatom content may be associated with a low charge efficiency. The latter is a key parameter for capacitive deionization and is defined as the ratio between the amounts of removed salt molecules and electrical charge.

Introduction

One of the key challenges our society is facing today is an increasing water demand caused by the rapid population growth over the last century. At the moment a variety of techniques are used for desalination namely distillation (DI),[1] reverse osmosis (RO),[2] and electrodialysis (ED).[3] Capacitive deionization (CDI) has gained considerable attention over the last ten years as an alternative desalination process.[4] CDI is especially attractive if brackish water is desalinated since it offers lower energy consumption compared to DI and RO processes where the continuous water phase is removed instead of merely the ions.[5]
CDI is based on the same principle as electrical double-layer capacitors (EDLC, also known as supercapacitors)[6] to desalinate water by storing ions in the electric double-layer on high surface area materials.[4, 7-11] The majority of CDI devices use high surface area porous carbon electrodes and a variety of carbon materials have been investigated so far, such as activated carbons,[12-14] mesoporous carbons,[15-17] carbon aerogels,[18-23] carbon nanotubes,[24-27] graphene,[28, 29] and carbide-derived carbons (CDC).[30, 31] Within the listed classes of carbons, optimized CDCs show a particularly narrow pore size distributions (PSD) which has helped tremendously to unravel the correlation between PSD and salt adsorption capacity.[30]
With regard to the limits in electrical conductivity and wettability of carbon materials, it is very attractive to explore incorporation of heteroatoms. Although electrical conductivity and wettability can be modified and enhanced, the presence of redox-active heteroatoms may additionally give rise to parasitic faradaic reactions. While the latter may be used to boost the specific capacitance of supercapacitors yielding improved energy storage performance,[32, 33] the situation is quite different for CDI. This is related to the salt removal process which is based on ion electrosorption and every Coulomb of charge not participating in the formation of an electrical double-layer, but instead in faradaic reactions, may ultimately decreases the charge efficiency (i.e., ratio of adsorbed salt and consumed charge). A clear exception can be found for very specific electrochemical systems, for example hybrid CDI[34] or desalination battery[35], that specifically employ redox reactions that involve salt ions.
In order to study such effects, materials with tailored chemical composition are required. For example, heteroatom doping is not accessible with CDC and also other top-down processes typically used for the synthesis of microporous carbons (such as chemical or physical activation of activated carbon) do not allow the controlled definition of heteroatoms. Therefore, a novel bottom-up salt template approach was used to synthesize microporous carbons with different heteroatom dopants (e.g., nitrogen or sulfur) with high yields at low costs.
We have recently demonstrated carbonization of ionic liquids (IL) in the presence of ordinary, low melting-point, inert salt mixtures serving as template and solvent at the same time.[36] Such an approach has unique advantages over classic templating syntheses. Firstly, the template itself is readily used and does not require a separate time step of template synthesis (like, for example, needed for silica templates).[37] Secondly, the template can either be removed by evaporation during the synthesis or it can be simply removed with water, thus highly toxic substances, such as HF or NH_4HF_2, are not required. Importantly and in contrast to the so-called $ZnCl_2$ activation used for the synthesis of activated carbons,[38] here we have a bottom-up generation of carbon from solution, which allows for design of the chemical composition in terms of heteroatom content of the final product.
In this study, we report for the first time the CDI performance of nanoporous heteroatom-doped carbons derived by a modified salt templating approach, herein extended to cheap and sustainable biomass based carbon precursors, such as glucose and glucosamine with 2-thiophenecarboxylic acid (TCA) as sulfur source. In addition to zinc chloride, cesium acetate was chosen as concurrent salt template and activating agent. It was previously demonstrated that cesium acetate can be used as a solvent and porogen for the polymerization of acrodam.[39] The carbon materials used in this study show high surface areas of up to 2830 m^2/g and varying heteroatom contents. Six different carbons with high fractions of microporosity have been selected to investigate the influence of heteroatom dopants on the charge efficiency in the CDI process. Additionally, the data is compared to the performance of a conventional activated carbon to

[1] *INM - Leibniz Institute for New Materials, Campus D2 2, 66123 Saarbrücken, Germany*
[2] *Max Planck Institute of Colloids and Interfaces, Colloids Department, Am Mühlenberg 1, 14476 Potsdam, Germany*
[3] *Saarland University, Campus D2 2, 66123 Saarbrücken, Germany*

[*] *Corresponding authors.*
eMail Tim Fellinger: fellinger@mpikg.mpg.de,
eMail Volker Presser: volker.presser@inm-gmbh.de

illustrate the universality of our findings on the role of heteroatoms on the CDI performance.

Results and Discussion

Structure of the synthetized carbon materials

When searching for alternative and cheaper precursors than ionic liquids, we found that metal chloride hydrate melts (esp. $ZnCl_2 \cdot 4\,H_2O$) act as effective solvents for otherwise hardly soluble carbohydrates like cellulose.[40, 41] At elevated temperatures it even catalyzes the dehydration of carbohydrates and therefore supports carbonization.[42] Dissolution of the carbon precursors (e.g. glucose and TCA for the synthesis of S-doped carbons) in an aqueous solution of $ZnCl_2$ ensures molecular mixing. In contrast to post-modification with heteroatoms here the growing carbon network is provided with a homogenous distribution of heteroatoms.

Throughout the synthesis water is evaporating to first form a $ZnCl_2$ hydrate melt (at 100 °C) and simultaneously at elevated temperatures, due to further evaporation, a $ZnCl_2$ melt, both acting as solvent and template. Also, usage of eutectic salt mixtures such as $LiCl/ZnCl_2$ or $KCl/ZnCl_2$ has an influence on generation of porosity, but was so far only reported for ionic liquid precursors or for non-doped carbons starting from biomass.[36, 43] The herein discussed samples will be denoted as C-Zn, NDC-Zn, SDC-Zn and NDC-Cs (Zn: $ZnCl_2$; Cs: cesium acetate, (N)(S)DC: nitrogen or sulfur doped carbon, C: carbon). The carbonization temperature used will be indicated in the end of the sample name while for the conventional activated carbon we used its commercial name (CWZ-22; see experimental description and *Supporting Information* **Fig. S1** for SEM images). Scanning electron microscopy (SEM) was used to investigate the particle structure of the as obtained carbons (**Fig. 1**).

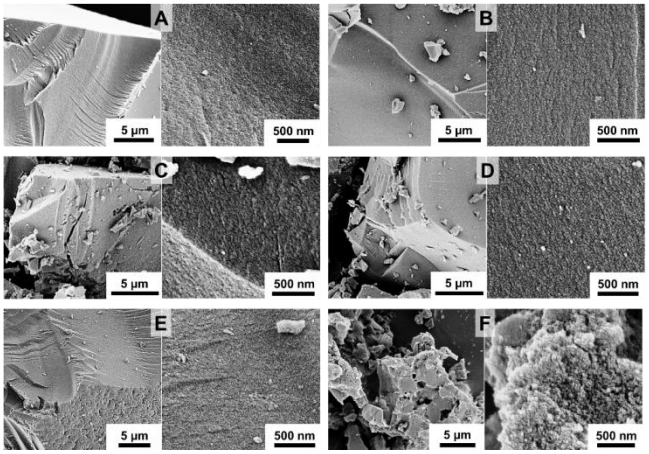

Figure 1. SEM images of (A) C-Zn-900, (B) NDC-Zn-800, (C) NDC-Zn-900, (D) NDC-Zn-1000, (E) SDC-Zn-900, and (F) NDC-Cs-900.

SEM reveals a compact product composed of large, highly porous particles for all the $ZnCl_2$ derived and differently doped carbons. Especially in case of NDC-Zn-1000 (**Fig. 1D**) one can observe, that the large particles are composed of strongly aggregated nanodomains. The interstitial gaps are formed by the molten salt phase, which is separated from the carbon phase throughout carbonization. Evaporation of the salt finally generates porosity. In the case where cesium acetate was used as additional and sacrificial template the structure is different. The large particles are cleft into smaller particles and also the primary particles are less aggregated, and give rise to extended porosity through additional mesopores. The morphology speaks for vast gas generation throughout the decomposition of cesium acetate, which disintegrates the otherwise observed morphology. Yet, all salt templated carbons were partially graphitic with a well-distinct D- and G-mode seen with Raman spectroscopy and a broadened (002)-peak seen around 26° 2θ with X-ray diffraction (see **Fig. S2**, *Supporting Information*). Nitrogen sorption experiments show, in general, a type I isotherm for the studied carbons (see **Fig. S3**, *Supporting Information*). The different mechanisms of surface area generation obviously lead to different pore structures and we see a significant difference in the amount and distribution of micro- and mesopores for the studied samples (**Fig. 2**). Values for the total specific surface area are as high as 1230 m^2/g and 2830 m^2/g for C-Zn-900 and NDC-Cs-900, respectively, with a high fraction of micropores, see **Fig. 2A** and **Fig. 2B**. Sulfur and nitrogen doped samples derived with $ZnCl_2$ showed a specific surface area of ~850 m^2/g, with a noticeable portion of micropores varying between 75-84 % of the total pore volume in case of SDC-Zn-900 and NDC-Zn-800, respectively. The higher surface area and the lower nitrogen content for NDC-Cs-900 compared to NDC-Zn-900 illustrates the top-down activation process in addition to the salt template generated porosity. Additionally, commercial activated carbon CWZ-22 exhibits a total pore volume of 0.65 cm^3/g composed mostly of micropores (**Table 1**).

Table 1. Elemental analysis and nitrogen sorption data for the synthesized carbons. Oxygen content is calculated as a difference between a total mass percentage and a sum of other heteroatoms listed below in the table. Dashes (-) indicate elemental concentration below the detection limit of the system (ca. 0.5 mass%).

Sample	Chemical analysis (mass%)				Residual (mass%)	Specific surface area (m^2/g)		Pore volume (cm^3/g)
	C	H	N	S	O	SSA_{BET}	SSA_{QSDFT}	V_{total}
C-Zn-900	94.3	1.1	-	-	4.6	1230	1110	0.65
NDC-Zn-900	77.1	2.9	5.4	-	14.6	840	780	0.36
SDC-Zn-900	92.1	1.6	-	2.0	4.3	885	830	0.38
NDC-Cs-900	85.0	1.5	1.0	-	12.5	2830	2110	1.56
NDC-Zn-800	60.2	2.7	5.7	-	31.5	880	860	0.45
NDC-Zn-1000	69.1	2.0	6.2	-	22.8	850	740	0.47
CWZ-22	86.4	-	-	-	12.6	880	941	0.45

Besides differences in pore structure, the carbon materials investigated in this study also varied greatly in the content and composition of non-carbon elements as needed for an investigation of the influence of heteroatom carbons. **Table 1** also shows wide variety of residual masses (very likely corresponding to the oxygen content) calculated as a difference between total mass percentage and sum of other heteroatom

contents such as nitrogen, sulfur, carbon, and hydrogen. We can also see that pore structure of nitrogen enriched carbons, except for NDC-Cs-900, shows only minor differences in terms of specific surface area, SSA_{BET}, total pore volume, V_{total}, and pore size distribution, see also **Fig. 2.**

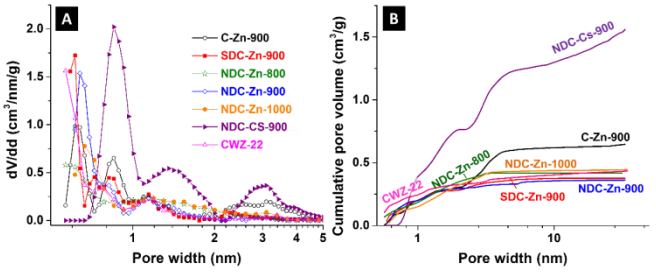

Figure 2. (A) Differential and (B) cumulative pore size distribution of heteroatom carbons and commercial CWZ-22 measured with nitrogen gas sorption at -196 °C and deconvoluted using quenched-solid density functional theory (QSDFT) kernel assuming slit-shaped pores.

The carbonization process presented in this work can be regarded as an equivalent process to the well-known hydrothermal carbonization (HTC) and concepts known from HTC may be easily adapted (e.g., achievement of sulfur doping).[44] In fact, using TCA as sulfur source together with glucose leads to carbons with 2 mass% of S and similar macroscopic morphology as compared to the non-sulfur doped carbons (see **Fig. 1**). The same applies for the synthesis of nitrogen doped carbons starting from glucosamine with a final 5.4 mass% of N (see **Table 1**). It is known that cesium acetate undergoes a thermal decomposition to Cs_2O.[45] The decomposition is likely accompanied by the evolution of CO_2, which leads to additional *in situ* activation of the as formed carbon material by means of the Boudouard equilibrium. Therefore, changing the salt template to cesium acetate leads to a strongly decreased yield and nitrogen content due to carbon etching. The carbon yield for the synthesis in $ZnCl_2$ is ~80 %, whereas it is reduced to ~50 % by using cesium acetate. If $ZnCl_2$ is used, the template is evaporated throughout the synthesis ($T_b(ZnCl_2)$=732 °C). This was confirmed by X-ray diffraction measurements (see **Fig. S1B**), which show the absence of peaks associated with any crystalline phase (such as $ZnCl_2$) and otherwise exclusively the reflections typical for amorphous carbon with the usual broad peaks originating from graphitic intra- and interlayer ordering.

Capacitive desalination performance

This section presents results for equilibrium salt adsorption, charge storage, and charge efficiency obtained using carbons doped with nitrogen or sulfur and characterized by different levels of oxygen content. In a first step, it is important to evaluate the charge storage capacity of the electrode material as obtained by plotting the accumulated charge versus the cell voltage (**Fig. 3A**). Interestingly, we find that the charge storage capacity of the studied salt templated carbons shows only minor differences, with values ranging from 20.0-22.5 C/g at 1.2 V. These values correspond to a specific capacitance of 67-75 F/g, when normalized to one single electrode active material as common in the supercapacitor community.[46] An exception is NDC-Cs-900, which shows a significantly higher charge storage capacity of ~40 C/g (= 132 F/g). It is very important to note that these values were obtained at low ionic strength (5 mM) and are, thus, not comparable for the use in supercapacitors where typically 1 M ionic strength (or higher) is employed; as it is well-known, the specific capacitance increases with molar concentration.[4] The high charge storage capacity of this material can be attributed to a significantly higher surface area (SSA_{BET}=2830 m^2/g as compared to <1500 m^2/g for all other carbons) and is in line with results presented in Ref. [30] for a comprehensive review of the CDI performance of a plethora of carbon materials with different porosity.

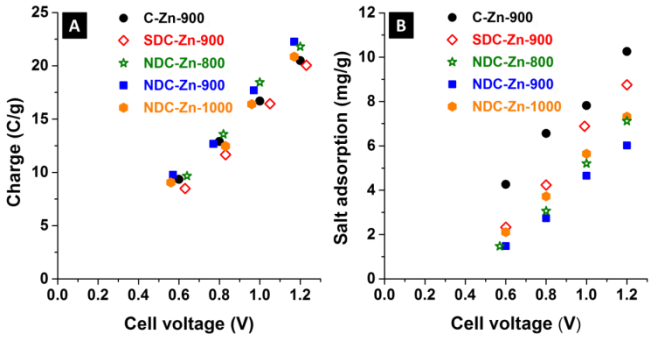

Figure 3. (A) Equilibrium charge and (B) equilibrium salt adsorption as function of cell voltage for carbons synthesized via salt template method expressed per gram of porous carbon in both electrodes. Data presented in these figures were obtained using salt concentration c_{salt}=5 mM of NaCl and single-pass method.

Just like charge, also the amount of accumulated salt depends on the cell voltage. As seen in **Fig. 3B**, the salt adsorption shows a much larger range of measured values depending on the used carbon material (again without considering NDC-Cs-900). This means that there is a disparity between the capacity for salt sorption and accumulated (invested) electrical charge. In more detail, salt sorption values at V_{cell}=1.2 V vary between 6 mg/g and 10 mg/g with the lowest value measured for NDC-Zn-900 and the highest for C-Zn-900. In accordance to the charge storage NDC-Cs-900 shows a higher salt adsorption capacity of ~15 mg/g, (=13.5 mg/g per total mass of both electrodes when including the binder), at 1.2 V in 5 mM NaCl. It is important to note that the value of 13.5 mg/g is amongst the highest values reported so far for porous carbons; in particular, it is comparable with optimized activated carbon (14.3 mg/g),[30] and multi-wall carbon nanotube/poly(vinyl alcohol) nanocomposite (13.1 mg/g)[47] and higher than graphene aerogel (9.9 mg/g at c_{salt}~ 10 mM)[48], and hierarchical porous CDC (12.8 mg/g).[30]

As a general trend, values from **Fig. 4** are in agreement with the measured pore structure. In particular, we have plotted a parity chart of measured versus predicted salt adsorption capacity adopting the predictive CDI performance evaluation introduced

in Ref. [30] (i.e., salt adsorption capacity analysis). In short, we used the cumulative pore size distribution data (**Fig. 2**) and pore-size-dependent salt adsorption capacities (also taken from Ref. [30]). In the case of salt templated carbons, this prediction may serve only as a rough estimate and we see significant deviations from the predicted performance (especially when comparing with literature data, as seen from **Fig. 4**). The direction of this systematic deviation is surprising: we predict a lower salt sorption capacity as it is actually measured for all samples except NDC-Zn-900. The latter ideally reproduces the actual prediction of CDI performance per pore size distribution analysis. For comparison, we see that the data point for the commercial carbon CWZ-22 falls below the prediction line, meaning that this material shows a performance which is lower than predicted by its pore structure. Based on the above analysis we recommend caution with (over)interpreting these data because of still unknown effects of surface heteroatoms.

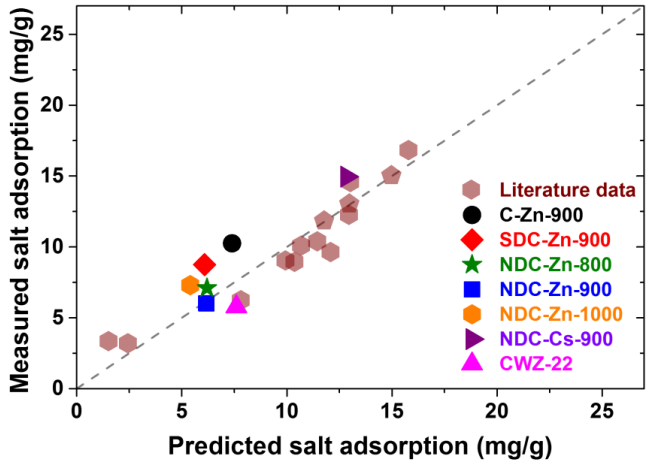

Figure 4. Measured versus calculated CDI performance of the samples used in this study using the porosity deconvolution method of Ref. [30]. The data points labelled "literature data" are also taken from Ref. [30].

The intriguing disparity between charge and ion storage must have a strong impact on the resulting charge efficiency, that is, how efficiently electric charge is used to remove salt from the aqueous electrolyte. As reported in Ref. [49], the theoretical limit of maximum charge efficiency is below unity; with experimental data reaching around 0.9-0.95 for membrane capacitive deionization[50] As such, the ideal case with a charge efficiency of unity, dictates that a material with a specific capacitance of 120 F/g measured using salt concentration of c_{salt}=5 mM NaCl at V_{cell}=1.0 V would achieve a maximum salt sorption capacity of ca. 22 mg/g. This simplistic calculation assumes that all the electric charge stored by carbon matrix is invested to adsorb one salt ion at any of the two electrodes. In reality, simultaneously with counterion adsorption, also co-ions are being expelled from the electrical double-layer formed at the carbon matrix-electrolyte interface. This process, depending on the actual salt concentration, lowers the resulting charge efficiency and values around 0.75-0.85 in c_{salt}=5 mM NaCl solution at V_{cell}=1.0 V are reported.[49] As a result, a more realistic upper limit for the maximum salt adsorption capacity is expected to be around 18 mg/g. These boundary parameters need to be considered for the discussion of the charge efficiency, as done in the next paragraphs.

In **Fig. 5** we show data for the charge efficiency obtained from equilibrium data as a function of the applied cell voltage. We note that C-Zn-900 as a non-doped carbon material with particularly low oxygen content (i.e., <5 mass%) shows the highest charge efficiency of around 0.85, while the lowest charge efficiencies are 0.45 found for NDC-Zn-900 with only 77.1 mass% carbon and 0.51 for NDC-Zn-800 with 60.2 mass% carbon (all data at 1.2 V). Also, as well-known from literature, all samples show a common relation between charge efficiency and cell voltage: the higher the cell voltage, the higher the charge

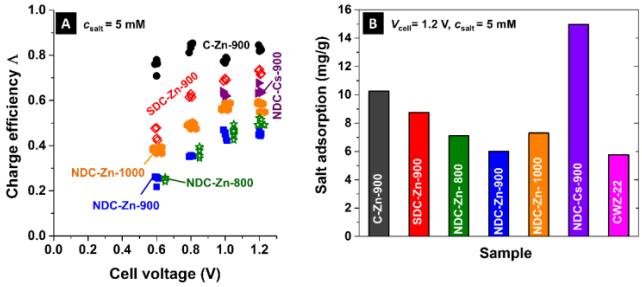

efficiency. The latter is a result from the transition between ion swapping (without actual bulk desalination) and preferential counter-ion adsorption with increased cell voltage (see Ref. [10] for a more detailed discussion).

Figure 5. (A) Charge efficiency as function of cell voltage and (B) maximum salt adsorption capacity at c_{salt}=5 mM and V_{cell}=1.2 V for carbons synthesized via salt template method and commercial CWZ-22. Salt adsorption is normalized to the mass of carbon without binder.

Most commonly, charge storage capacity is related with two parameters, namely porosity characteristics and surface functionalization / chemical composition. Yet, as seen from the data presented before, all structural parameters such as specific surface area, SSA_{BET}, total pore volume, V_{total}, and pore size distribution of the tested materials are very comparable with the exception of C-Zn-900 and NDC-Zn-900; yet, the charge efficiency values still vary greatly between 0.45 and 0.72. Considering recent studies (namely, Ref. [30] and Ref. [31]), the charge efficiency is only marginally influenced by the pore size distribution, leaving the chemical composition as the most likely parameter affecting the charge efficiency.

In **Fig. 6A** we show the relationship between elemental carbon content and the measured charge efficiency. Values below 100 % carbon content represent the cumulative contribution of hydrogen, nitrogen, sulfur, and residual mass (per our elemental analysis; see **Fig. 6B** and **Table 1**). Typically, the residual mass equals the oxygen content; however especially for nitrogen doped samples some additional zinc can be present, due to coordination of zinc ions to the nitrogen sites. From these data, we see a general trend: higher charge efficiency for samples with higher carbon contents. A minimum plateau region of charge efficiency between 0.45 and ~0.6 is characteristic for electrodes with carbon content lower than 80 mass%. We also

note that in case of CWZ-22, the charge efficiency is as low as 0.45, even though the carbon content is equal to 86 mass%. Such a low charge efficiency is not typical for activated carbons and typical values for well-performing materials are above 0.8 (depending on the operation mode and conditions also higher values are commonly found).[51] Thus, not just the mere presence of heteroatoms is important but the specific chemical group they are associated with is seemingly also playing a major role. A deeper analysis of this aspect is important for the advancement of the CDI technology but beyond the scope of this study.

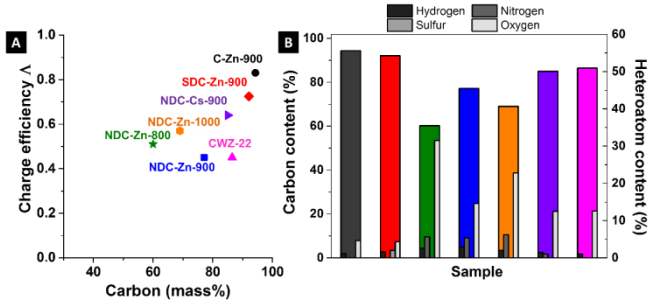

Figure 6. (A) Relation between charge efficiency at c_{salt}=5 mM and V_{cell}=1.2 V for all carbon electrodes tested in CDI as function of carbon content. (B) Chemical analysis of the carbon samples tested in CDI.

Still, based on data presented in **Fig. 6**, several conclusions can be drawn. For one, the presence of oxygen surface groups seems to be mainly responsible for a decrease of charge efficiency. This observation is supported by low charge efficiency of the CWZ-22 electrodes consisting of 86.4 mass% of carbon and 12.6 mass% of oxygen. The mass content of other heteroatoms such as nitrogen, sulfur, and hydrogen in this carbon is either very low or below the system's detection limit. Furthermore, nitrogen doped carbon electrodes such as NDC-Zn-800 and NDC-Zn-1000 contain an equivalent amount of nitrogen and hydrogen but different amount of oxygen. Considering that the charge efficiency of these two samples is rather similar, the oxygen content alone is obviously an insufficient measure for the charge efficiency and the type of oxygen surface groups may play a more important role.
Considering the limited use of infrared spectroscopy for highly porous carbon samples and the inaccessibility of the large surface area inside the carbon particles with X-ray photoelectron spectroscopy, we provide a first investigation of the role of surface functionality with streaming potential measurements of three selected carbons.

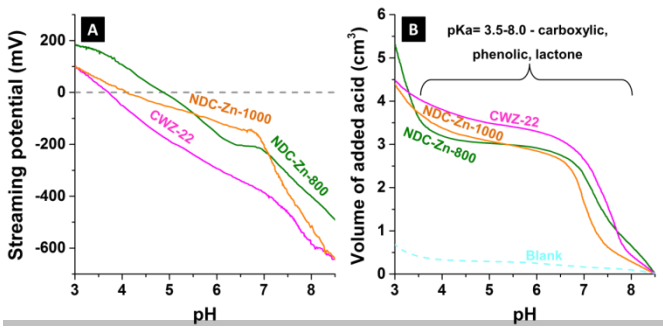

Figure 7. (A) Streaming potential curves for carbon samples with different doping levels and oxygen content. (B) Volume of hydrochloric acid, pH=1.6, used for streaming potential measurements.

Fig. 7A shows the relation between streaming potential and the pH-value of the solution. We see that the isoelectric point of nitrogen-doped carbon appears at pH of 4.9 and 4.1 for NDC-Zn-800 and NDC-Zn-1000, respectively, and the isoelectric point of CWZ-22 is located at a pH of 3.7. It is important to note that pKa values of oxygen surface groups such as carboxylic, phenolic and lactone are in the range of 3.5 and 8.0. Therefore, we can assume that most of these groups at starting pH of 8.5 are deprotonated and will become protonated with decreasing pH. **Fig. 7B** depicts the volume of the hydrochloric acid (pH=1.6) used during streaming potential measurements and we can see that CWZ-22 consumes the largest volume of acid. The latter indicates a higher surface charge even though the actual content of oxygen is lower compared with NDC-Zn-800 and NDC-Zn-1000 carbons. This result may explain why CWZ-22 has slightly lower charge efficiency than NDC-Zn-800 and NDC-Zn-1000, while its oxygen content is lower.

Conclusions

We have surveyed a novel class of nanoporous carbon materials synthesized via salt templating from abundantly available biomass as an electrode material for water desalination by capacitive deionization. Varying the synthesis conditions and the synthesis procedure, we obtained a range of carbon with and without heteroatoms, namely oxygen, sulfur and / or nitrogen. The latter two are currently extensively explored as a facile approach to enhance the performance of electrochemical energy storage devices, foremost supercapacitors. One of the investigated materials, namely NDC-Cs-900 (nitrogen-doped), yielded a high salt adsorption capacity of 15.0 mg/g at 1.2 V (5 mM NaCl) which is amongst the highest values reported so far.
Our study also shows that designing carbons with a high heteroatom content is not without complications and can cause severe limitations when considering the charge efficiency. The latter is a key performance parameter for overall energy consumption and the usually very high charge efficiency gives rise to the commonly high energy efficiency of CDI systems. Unlike the field of supercapacitors, CDI performance has to be evaluated always in two categories, namely the amount of electrosorbed salt ions and the amount of consumed electric charge to accomplish this feat. In particular, our best-performing carbon material NDC-Cs-900 exhibits a low charge efficiency of 0.64 at 1.2 V in 5 mM NaCl. This is severely lower than for carbons with a low carbon heteroatom content and we note that common conventional porous carbons (e.g., activated carbons) shows much higher values for the charge efficiency (typically >0.80). Thus, our study gives first insights to the importance of surface chemistry and the type of carbon heteroatoms on the CDI performance. A first indication of the central role of oxygen surface groups is provided by careful evaluation of the charge efficiency versus chemical composition and including a low-

performance commercial activated carbon with high carbon content. Streaming potential measurements indicate that the surface charge of carbons may play a key role in understanding the correlation between charge efficiency and chemical composition, but further work is needed to quantify and expand this aspect.

Experimental Section

Salt template synthesis of porous carbons

3 g of carbon precursor (i.e., glucose or glucosamine hydrochloride) were dissolved together with 3 g $ZnCl_2$ or 15 g of cesium acetate in 20 mL of deionized water. For the sulfur doped samples 250 mg of TCA were added to the precursor solution. The solution was subsequently transferred into a ceramic crucible and placed in a tube furnace (Carbolite CTF) under nitrogen flow. The atmosphere was conditioned for 20 min before a heating ramp of 1 °C/min was applied to 300 °C followed by 4.5 °C/min to the final carbonization temperature of 800, 900, or 1000 °C. After the oven was allowed to cool down to room temperature under nitrogen flow, the products were washed with water and dried at 80 °C in vacuum for 12 h to yield the porous, (heteroatom doped) carbons.

Physical characterization

Scanning electron microscopy (SEM) images were recorded on a Gemini Leo-1150 instrument with an acceleration voltage of 0.1 to 30 kV. The samples were prepared by placing the grounded carbon samples onto carbon tape and subsequent sputtering with Au/Pd. Transmission electron microscopy (TEM) images were recorded on a Philips CM200FEG microscope (200 kV) equipped with a field emission gun.

Nitrogen gas sorption measurements at -196 °C were carried out with an Autosorb iQ system (Quantachrome). The samples were outgassed at 150 °C for 10 h under vacuum conditions at 10^2 Pa to remove adsorbed water. Nitrogen gas sorption was performed in liquid nitrogen in the relative pressure range from $1 \cdot 10^{-7}$ to 1.0 in 68 steps. The specific surface area (SSA) was calculated with the ASiQwin-software using the Brunauer-Emmett-Teller (BET) equation [52] in the linear relative pressure range 0.01-0.2 (i.e., SSA_{BET}). We also calculated the SSA and pore size distribution (PSD) via quenched-solid density functional theory (QSDFT; i.e., SSA_{QSDFT}) with a hybrid model for slit and cylindrical pores and pore size between 0.56 and 37.5 nm.[53] The hybrid model yielded a better fit compared to a simple slit-shaped pore model. Values for the total pore volume correspond to p/p_0=0.95.

The elemental composition was determined by means of elemental analysis (EA) using a Vario El elemental analyzer for carbon, nitrogen, sulfur and hydrogen content. X-Ray diffraction (XRD) pattern were recorded using a Bruker D8 advance diffractometer with a Cu-K_α (λ=0.154 nm) radiation source and a step size of 0.1 °/s. Raman spectra were recorded with an inVia Renishaw system operating at 532 nm with 0.2 mW laser power focused with a 50x lens (numeric aperture: 0.75) and a spectral resolution of ca. 1.2 1/cm.

Streaming potential measurements, SPM, were conducted with a 0.5 mass% suspension of carbon particles in demineralized water at initial pH=8.5-9.0 using a particle charge detector (PCD-03, BGT Mütek, Switzerland). Before SPM measurements, the pH-value of each sample was adjusted by dosing small amount of 3 mass% of ammonia solution. Hydrochloric acid, HCl, with pH=1.6 was used as titrant.

Electrode preparation

Electrodes from six different salt templated porous carbons and one commercially available activated carbon (CWZ-22, Elbar Katowice) were prepared using procedure similar to that described in Ref. [54]. First, a porous carbon material (90 mass%) was mixed in a mortar with 10 mass% of dissolved polytetrafluoroethylene (PTFE, 60 mass% solution in water from Sigma Aldrich, USA) and ethanol to obtain homogeneous carbon paste. Next such a carbon paste was rolled with a rolling machine (MTI HR01, MIT Corp.) to a 150±20 mm thick free standing electrode and dried at 120 °C for 24 h. Before the CDI experiments were performed, the carbon electrodes were cut into square pieces of 6x6 cm^2 with a hole in the middle of each electrode of 1.5x1.5 cm^2. The final electrode mass density varied between 0.3 and 0.93 g/cm^3.

CDI experiments

A CDI setup similar to that described in Ref. [31] was used to characterize desalination properties of all carbon materials described in this work. The CDI stack was comprised of a graphite current collector (SGL Technologies, Germany; thickness: 220 □m) together with porous carbon electrodes and a porous spacer (glass fiber pre-filter, Millipore, compressed thickness of a single layer; thickness: 250 □m). More specifically, each current collector is used for two adjacent cells, except for the bottom and the top which in only in contact with one carbon electrode. After stack assembly, the stack with two parallel flow paths is firmly pressed together and sealed. A constant flow rate of Φ=7.5 mL/min per one flow channel is used throughout this work. Ion adsorption and desorption steps are carried out using constant potential mode at four different cell voltages, V_{cell}, applied to the cell during adsorption step, while discharge step is accomplished at V_{cell}=0 V. For all electrochemical operations, we used a VSP300potentiostat/galvanostat (Bio-Logic) and the duration of each half-cycle was 30 min. All experiments were carried out in c_{in}=5 mM NaCl solution and an electrolyte vessel which was flushed continuously with N_2 gas to purge the water from dissolved oxygen. The salt adsorption capacity and the measured charge are defined per mass of active material in both electrodes and are calculated as an average value from adsorption and desorption step. For calculating charge, the leakage current measured at the end of each half-cycle was subtracted.

Acknowledgements

The INM (www.inm-gmbh.de) is part of the Leibniz Research Alliance Energy Transition (LVE). SP acknowledges financial support by the Alexander-von-Humboldt Foundation. VP acknowledges funding from the Hans Meier Leibniz Award of the German Research Foundation (DFG). Marco Zeiger (INM) is kindly thanked for his support with Raman spectroscopy and scanning electron microscopy. SP, MA, and VP thank Prof. Eduard Arzt (INM) for his continuing support.

Keywords: capacitive deionization • salt templating • heteroatom carbon • charge efficiency • desalination

1. Alklaibi, A.; Lior, N. Membrane-distillation desalination: status and potential. *Desalination* 2005, 171, 111-131.

2. Fritzmann, C.; Löwenberg, J.; Wintgens, T.; Melin, T. State-of-the-art of reverse osmosis desalination. *Desalination* 2007, 216, 1-76.

3. Sadrzadeh, M.; Mohammadi, T. Sea water desalination using electrodialysis. *Desalination* 2008, 221, 440-447.

4. Porada, S.; Zhao, R.; Van Der Wal, A.; Presser, V.; Biesheuvel, P. Review on the science and technology of water desalination by capacitive deionization. *Progress in Materials Science* 2013, 58, 1388-1442.

5. Zhao, R.; Porada, S.; Biesheuvel, P. M.; van der Wal, A. Energy consumption in membrane capacitive deionization for different water recoveries and flow rates, and comparison with reverse osmosis. *Desalination* 2013, 330, 35-41.

6. Beguin, F.; Presser, V.; Balducci, A.; Frackowiak, E. Carbons and electrolytes for advanced supercapacitors. *Advanced Materials* 2014, 26, 2219 - 2251.

7. Biesheuvel, P. M.; van Limpt, B.; van der Wal, A. Dynamic Adsorption/Desorption Process Model for Capacitive Deionization. *The Journal of Physical Chemistry C* 2009, 113, 5636-5640.

8. Biesheuvel, P. M.; van der Wal, A. Membrane capacitive deionization. *Journal of Membrane Science* 2010, 346, 256-262.

9. Oren, Y. Capacitive deionization (CDI) for desalination and water treatment — past, present and future (a review). *Desalination* 2008, 228, 10-29.

10. Kim, T.; Dykstra, J. E.; Porada, S.; van der Wal, A.; Yoon, J.; Biesheuvel, P. M. Enhanced charge efficiency and reduced energy use in capacitive deionization by increasing the discharge voltage. *Journal of Colloid and Interface Science* 2015, 446, 317-326.

11. Mahmoud, K. A.; Mansoor, B.; Mansour, A.; Khraisheh, M. Functional graphene nanosheets: The next generation membranes for water desalination. *Desalination* 2015, 356, 208-225.

12. Zou, L.; Morris, G.; Qi, D. Using activated carbon electrode in electrosorptive deionisation of brackish water. *Desalination* 2008, 225, 329-340.

13. Oh, H. J.; Lee, J. H.; Ahn, H. J.; Jeong, Y.; Kim, Y. J.; Chi, C. S. Nanoporous activated carbon cloth for capacitive deionization of aqueous solution. *Thin Solid Films* 2006, 515, 220-225.

14. Seo, S. J.; Jeon, H.; Lee, J. K.; Kim, G. Y.; Park, D.; Nojima, H.; Lee, J.; Moon, S. H. Investigation on removal of hardness ions by capacitive deionization (CDI) for water softening applications. *Water Res.* 2010, 44, 2267-2275.

15. Tsouris, C.; Mayes, R.; Kiggans, J.; Sharma, K.; Yiacoumi, S.; DePaoli, D.; Dai, S. Mesoporous Carbon for Capacitive Deionization of Saline Water. *Environmental Science & Technology* 2011, 45, 10243-10249.

16. Li, L. X.; Zou, L. D.; Song, H. H.; Morris, G. Ordered mesoporous carbons synthesized by a modified sol-gel process for electrosorptive removal of sodium chloride. *Carbon* 2009, 47, 775-781.

17. Mayes, R. T.; Tsouris, C.; Kiggans, J. O.; Mahurin, S. M.; DePaoli, D. W.; Dai, S. Hierarchical ordered mesoporous carbon from phloroglucinol-glyoxal and its application in capacitive deionization of brackish water. *J. Mater. Chem.* 2010, 20, 8674-8678.

18. Jung, H. H.; Hwang, S. W.; Hyun, S. H.; Kang-Ho, L.; Kim, G. T. Capacitive deionization characteristics of nanostructured carbon aerogel electrodes synthesized via ambient drying. *Desalination* 2007, 216, 377-385.

19. Sui, Z. Y.; Meng, Q. H.; Zhang, X. T.; Ma, R.; Cao, B. Green synthesis of carbon nanotube-graphene hybrid aerogels and their use as versatile agents for water purification. *J. Mater. Chem.* 2012, 22, 8767-8771.

20. Farmer, J. C.; Fix, D. V.; Mack, G. V.; Pekala, R. W.; Poco, J. F. Capacitive deionization of NaCl and NaNO3 solutions with carbon aerogel electrodes. *J. Electrochem. Soc.* 1996, 143, 159-169.

21. Gabelich, C. J.; Tran, T. D.; Suffet, I. H. Electrosorption of inorganic salts from aqueous solution using carbon aerogels. *Environmental science & technology* 2002, 36, 3010-3019.

22. Xu, P.; Drewes, J. E.; Heil, D.; Wang, G. Treatment of brackish produced water using carbon aerogel-based capacitive deionization technology. *Water Research* 2008, 42, 2605-2617.

23. Yang, K.-L.; Ying, T.-Y.; Yiacoumi, S.; Tsouris, C.; Vittoratos, E. S. Electrosorption of Ions from Aqueous Solutions by Carbon Aerogel: An Electrical Double-Layer Model. *Langmuir* 2001, 17, 1961-1969.

24. Li, H.; Gao, Y.; Pan, L.; Zhang, Y.; Chen, Y.; Sun, Z. Electrosorptive desalination by carbon nanotubes and nanofibres electrodes and ion-exchange membranes. *Water Research* 2008, 42, 4923-4928.

25. Li, H. B.; Gao, Y.; Pan, L. K.; Zhang, Y. P.; Chen, Y. W.; Sun, Z. Electrosorptive desalination by carbon nanotubes and nanofibres electrodes and ion-exchange membranes. *Water Res.* 2008, 42, 4923-4928.

26. Gao, Y.; Pan, L. K.; Li, H. B.; Zhang, Y. P.; Zhang, Z. J.; Chen, Y. W.; Sun, Z. Electrosorption behavior of cations with carbon nanotubes and carbon nanofibres composite film electrodes. *Thin Solid Films* 2009, 517, 1616-1619.

27. Wang, L.; Wang, M.; Huang, Z. H.; Cui, T. X.; Gui, X. C.; Kang, F. Y.; Wang, K. L.; Wu, D. H. Capacitive deionization of NaCl solutions using carbon nanotube sponge electrodes. *J. Mater. Chem.* 2011, 21, 18295-18299.

28. Li, H.; Lu, T.; Pan, L.; Zhang, Y.; Sun, Z. Electrosorption behavior of graphene in NaCl solutions. *J. Mater. Chem.* 2009, 19, 6773-6779.

29. Li, H. B.; Zou, L. D.; Pan, L. K.; Sun, Z. Novel Graphene-Like Electrodes for Capacitive Deionization. *Environ Sci Technol* 2010, 44, 8692-8697.

30. Porada, S.; Borchardt, L.; Oschatz, M.; Bryjak, M.; Atchison, J.; Keesman, K.; Kaskel, S.; Biesheuvel, P.; Presser, V. Direct prediction of the desalination performance of porous carbon electrodes for capacitive deionization. *Energy & Environmental Science* 2013, 6, 3700-3712.

31. Porada, S.; Weinstein, L.; Dash, R.; van der Wal, A.; Bryjak, M.; Gogotsi, Y.; Biesheuvel, P. M. Water Desalination Using Capacitive Deionization with Microporous Carbon Electrodes. *ACS Applied Materials & Interfaces* 2012, 4, 1194-1199.

32. Fujisawa, K.; Cruz-Silva, R.; Yang, K.-S.; Kim, Y. A.; Hayashi, T.; Endo, M.; Terrones, M.; Dresselhaus, M. S. Importance of open, heteroatom-decorated edges in chemically doped-graphene for supercapacitor applications. *Journal of Materials Chemistry A* 2014, 2, 9532-9540.

33. Chen, L.-F.; Huang, Z.-H.; Liang, H.-W.; Gao, H.-L.; Yu, S.-H. Three-Dimensional Heteroatom-Doped Carbon Nanofiber Networks Derived from Bacterial Cellulose for Supercapacitors. *Advanced Functional Materials* 2014, 24, 5104-5111.

34. Lee, J.; Kim, S.; Kim, C.; Yoon, J. Hybrid capacitive deionization to enhance the desalination performance of capacitive techniques. *Energ Environ Sci* 2014, 7, 3683-3689.

35. Pasta, M.; Wessells, C. D.; Cui, Y.; La Mantia, F. A Desalination Battery. *Nano Letters* 2012, 12, 839-843.

36. Fechler, N.; Fellinger, T. P.; Antonietti, M. “Salt Templating”: A Simple and Sustainable Pathway toward Highly Porous Functional Carbons from Ionic Liquids. *Advanced Materials* 2013, 25, 75-79.

37. Zhao, D. Y.; Feng, J. L.; Huo, Q. S.; Melosh, N.; Fredrickson, G. H.; Chmelka, B. F.; Stucky, G. D. Triblock copolymer syntheses of mesoporous silica with periodic 50 to 300 angstrom pores. *Science* 1998, 279, 548-552.

38. Molina-Sabio, M.; Rodríguez-Reinoso, F. Role of chemical activation in the development of carbon porosity. *Colloids and Surfaces A: Physicochemical and Engineering Aspects* 2004, 241, 15-25.

39. Chung, K. K.; Fechler, N.; Antonietti, M. A Salt-Flux Synthesis of Highly Porous, N- and O-Doped Carbons from a Polymer Precursor and Its Use for High Capacity/High Rate Supercapacitors. *Advanced Porous Materials* 2014, 2, 61-68.

40. Fischer, S.; Leipner, H.; Thümmler, K.; Brendler, E.; Peters, J. Inorganic molten salts as solvents for cellulose. *Cellulose* 2003, 10, 227-236.

41. Leipner, H.; Fischer, S.; Brendler, E.; Voigt, W. Structural changes of cellulose dissolved in molten salt hydrates. *Macromolecular Chemistry and Physics* 2000, 201, 2041-2049.

42. Deng, T.; Cui, X.; Qi, Y.; Wang, Y.; Hou, X.; Zhu, Y. Conversion of carbohydrates into 5-hydroxymethylfurfural catalyzed by ZnCl2 in water. *Chemical Communications* 2012, 48, 5494-5496.

43. Ma, Z.; Zhang, H.; Yang, Z.; Zhang, Y.; Yu, B.; Liu, Z. Highly mesoporous carbons derived from biomass feedstocks templated with eutectic salt ZnCl2/KCl. *Journal of Materials Chemistry A* 2014, 2, 19324-19329.

44. Wohlgemuth, S.-A.; White, R. J.; Willinger, M.-G.; Titirici, M.-M.; Antonietti, M. A one-pot hydrothermal synthesis of sulfur and nitrogen doped carbon aerogels with enhanced electrocatalytic activity in the oxygen reduction reaction. *Green Chemistry* 2012, 14, 1515.

45. Meyer, U.; Gorzawski, H.; Hölderich, W. F. Michael addition of ethyl acrylate and acetone over solid bases. *Catalysis Letters* 1999, 59, 201-206.

46. Zhang, S.; Pan, N. Supercapacitors Performance Evaluation. *Advanced Energy Materials* 2014, n/a-n/a.

47. Hou, C.-H.; Liu, N.-L.; Hsu, H.-L.; Den, W. Development of multi-walled carbon nanotube/poly(vinyl alcohol) composite as electrode for capacitive deionization. *Separation and Purification Technology* 2014, 130, 7-14.

48. Yin, H.; Zhao, S.; Wan, J.; Tang, H.; Chang, L.; He, L.; Zhao, H.; Gao, Y.; Tang, Z. Three-Dimensional Graphene/Metal Oxide Nanoparticle Hybrids for High-Performance Capacitive Deionization of Saline Water. *Advanced Materials* 2013, 25, 6270-6276.

49. Biesheuvel, P. M.; Porada, S.; Levi, M.; Bazant, M. Z. Attractive forces in microporous carbon electrodes for capacitive deionization. *J Solid State Electr* 2014, 18, 1365-1376.

50. Zhao, R.; Biesheuvel, P. M.; Van der Wal, A. Energy Consumption and Constant Current Operation in Membrane Capacitive Deionization. *Energy & Environmental Science* 2012, 5, 9520-9527.

51. Kim, T.; Dykstra, J. E.; Porada, S.; van der Wal, A.; Yoon, J.; Biesheuvel, P. M. Enhanced charge efficiency and reduced energy use in capacitive deionization by increasing the discharge voltage. *Journal of Colloid and Interface Science* 2014.

52. Brunauer, S.; Emmett, P. H.; Teller, E. Adsorption of Gases in Multimolecular Layers. *Journal of the American Chemical Society* 1938, 60, 309-319.

53. Gor, G. Y.; Thommes, M.; Cychosz, K. A.; Neimark, A. V. Quenched solid density functional theory method for characterization of mesoporous carbons by nitrogen adsorption. *Carbon* 2012, 50, 1583-1590.

54. Jäckel, N.; Weingarth, D.; Zeiger, M.; Aslan, M.; Grobelsek, I.; Presser, V. Comparison of carbon onions and carbon blacks as conductive additives for carbon supercapacitors in organic electrolytes. *Journal of Power Sources* 2014, 272, 1122-1133.